



Visualizing the very-large-scale motions in turbulent pipe flow

Leo H. O. Hellström, Aman Sinha, and Alexander J. Smits

Citation: *Physics of Fluids* **23**, 011703 (2011); doi: 10.1063/1.3533016

View online: <http://dx.doi.org/10.1063/1.3533016>

View Table of Contents: <http://scitation.aip.org/content/aip/journal/pof2/23/1?ver=pdfcov>

Published by the [AIP Publishing](#)

Articles you may be interested in

[Comparison of large- and very-large-scale motions in turbulent pipe and channel flows](#)

Phys. Fluids **27**, 025101 (2015); 10.1063/1.4906805

[Comparison of very-large-scale motions of turbulent pipe and boundary layer simulations](#)

Phys. Fluids **25**, 045103 (2013); 10.1063/1.4802048

[Measurement of turbulent flow upstream and downstream of a circular pipe bend](#)

Phys. Fluids **24**, 041702 (2012); 10.1063/1.4704196

[Very large-scale motion in the outer layer](#)

Phys. Fluids **11**, 417 (1999); 10.1063/1.869889

[Planar visualizations of large-scale turbulent structures in axisymmetric supersonic separated flows](#)

Phys. Fluids **11**, 201 (1999); 10.1063/1.869913



The Unveiling Nears

The new *Physics Today* website will soon be launched. It will be faster, more attractive, and easier to search on all your devices.

**PHYSICS
TODAY**

Visualizing the very-large-scale motions in turbulent pipe flow

Leo H. O. Hellström,^{a)} Aman Sinha, and Alexander J. Smits^{b)}
*Department of Mechanical and Aerospace Engineering, Princeton University,
 Princeton, New Jersey 08544, USA*

(Received 7 October 2010; accepted 8 December 2010; published online 26 January 2011)

Time-resolved stereoscopic particle image velocimetry is used to investigate the structure of the very-large-scale motions (VLSMs) in fully developed turbulent pipe flow. The motions are visualized using snapshot proper orthogonal decomposition. It is shown that the structures can be reconstructed using a small number of the most energetic modes. The results strongly suggest a possible connection between the origin of the VLSM and linear stability analysis. The structures are seen to be highly three-dimensional, meandering azimuthally and radially. At this Reynolds number ($Re_D=12\,500$), they occasionally extend from the near-wall region to the wake region of the pipe. © 2011 American Institute of Physics. [doi:10.1063/1.3533016]

Very long, meandering features consisting of narrow regions of low streamwise momentum fluid, flanked by regions of higher momentum fluid, have been observed in the logarithmic and wake regions of wall flows.^{1–5} In internal flows, the motions are referred to as very-large-scale motions (VLSMs), whereas in external flows they are known as “superstructures.” Measurements in channels and pipes have found VLSM as long as 30 times the channel half-height h or pipe radius R ,⁶ while experiments in boundary layers show instances of superstructures with lengths up to 10–15 times the boundary layer thickness δ .⁷ For internal geometries the VLSMs are found to persist well into the outer layer,⁸ whereas the superstructures in boundary layers appear to be limited to the logarithmic region,⁹ although recent work has found evidence of weak elongated structures within boundary layers out to the edge of the layer.¹⁰

These very-large-scale features are important in that they make a significant contribution to the turbulent kinetic energy and Reynolds stress production. For example, Balakumar and Adrian¹ found that 40%–65% of the kinetic energy and 30%–50% of the Reynolds shear stress are accounted for in the long modes with streamwise wavelengths greater than 3δ . Furthermore, these structures have large radial scales that modulate the near-wall flow, which helps to explain Reynolds number dependent variations in the near-wall Reynolds stress distributions.^{7,11,12}

The origin of the VLSM and superstructures is not yet clear. It has been proposed that the VLSM may be caused by pseudostreamwise alignment of the large-scale motions,³ but it has also been suggested that they could be formed by linear processes.^{13,14} In particular, the first VLSM-type (linear) response mode reveals streamwise velocity structures about $3R$ long,¹⁴ and a superposition of two additional response modes reproduces the observed meandering coherence of the order of $25R$.¹⁵

Here, we visualize the VLSMs in moderate Reynolds number pipe flows using time-resolved stereoscopic particle

image velocimetry (SPIV). Snapshot proper orthogonal decomposition (POD) of the three-dimensional fluctuating velocity field is used to filter the data and extract the VLSMs. The results give strong support for the hypothesis by McKeon and Sharma that highly selective linear mechanisms are important to the origin of VLSMs.¹⁴

The flow facility consists of a 20 m long clear polyvinyl chloride pipe of diameter $D=40$ mm with a glass test section located $150D$ downstream of the pipe entrance. Water is used as the working fluid. A Plexiglas box filled with glycerin surrounds the test section to minimize optical distortion due to refraction through the pipe wall, as shown in Fig. 1.

The SPIV data were acquired using a single Redlake MotionXtra HG-LE camera (up to 1200 fps when using a resolution of 1040×640 pixels). The water was seeded with $100\ \mu\text{m}$ diameter neutrally buoyant particles. The maximum Reynolds number is limited to 35 000 because at higher velocities the particles begin to leave the 1.5 mm thick laser sheet during the minimum image pair time interval. The results presented here were obtained at a Reynolds number $Re_D=12\,500$, where $Re_D=D\langle U\rangle/\nu$, $\langle U\rangle$ is the bulk velocity, and ν is the kinematic viscosity. Previous measurements conducted in pipe flow showed that the shape and size of the VLSM are relatively insensitive to Reynolds number.⁸

In every exposure, the camera records two separate images, each comprising a 45° view of the test section interrogation plane (see Fig. 1). After each image pair has been separately processed using standard PIV software, the particle displacement fields are mapped into a circular shape using a fourth-order polynomial. The two displacement fields are then fitted onto a common, denser grid using a triangle-based cubic interpolation method. Each data point has one displacement component from both camera views and can then be reconstructed into a three component displacement field according to

$$\Delta x = \frac{\Delta x_2}{\cos \alpha_2} \left[1 - \frac{\cos \alpha_1 \sin \alpha_2}{\sin(\alpha_1 + \alpha_2)} \right] - \frac{\Delta x_1}{\cos \alpha_1} \left[\frac{\cos \alpha_1 \sin \alpha_2}{\sin(\alpha_1 + \alpha_2)} \right], \quad (1)$$

^{a)}Electronic mail: lhellstr@princeton.edu.

^{b)}Electronic mail: asmits@princeton.edu.

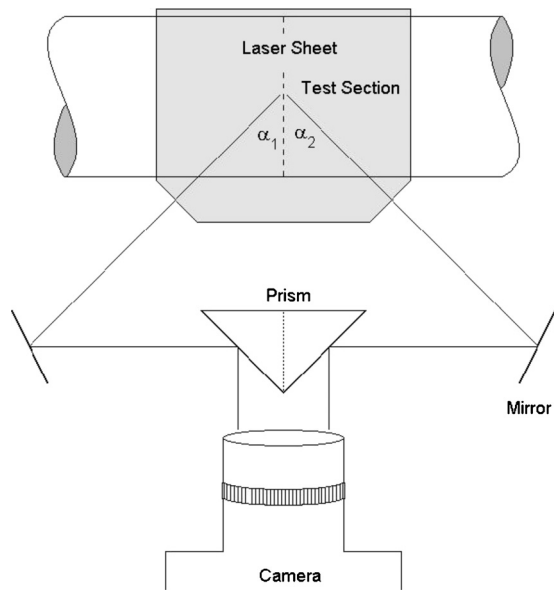


FIG. 1. Optical setup for the single-camera SPIV system.

$$\Delta y = \frac{\Delta y_1 + \Delta y_2}{2}, \tag{2}$$

$$\Delta z = \frac{\Delta x_2}{\cos \alpha_2} \left[\frac{\cos \alpha_1 \cos \alpha_2}{\sin(\alpha_1 + \alpha_2)} \right] + \frac{\Delta x_1}{\cos \alpha_1} \left[\frac{\cos \alpha_1 \cos \alpha_2}{\sin(\alpha_1 + \alpha_2)} \right], \tag{3}$$

where indexes 1 and 2 represent the left and right viewing angles, respectively. Here, Δx , Δy , and Δz are the streamwise, vertical, and horizontal displacement components, respectively. The velocity components in a Cartesian coordinate system are then found by dividing the displacement components by the time delay between successive images. Also, α is the angle from the wall normal to the camera view, Δx_1 and Δx_2 are the horizontal displacements calculated from the image-halves, while Δy_1 and Δy_2 are the corresponding vertical displacements. The general approach is based on the methodology presented by van Doorne and

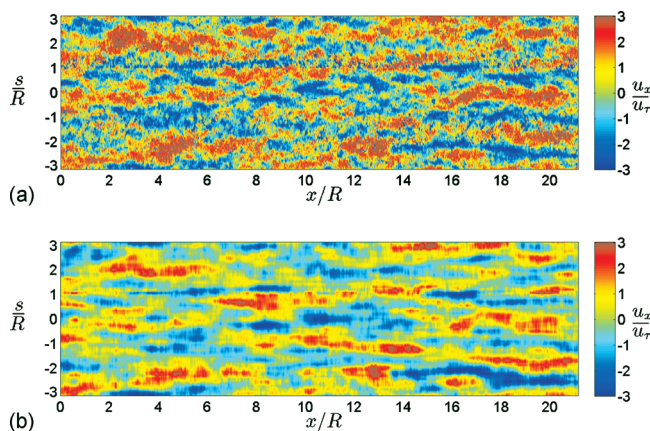


FIG. 2. (Color) Contour plots of the streamwise velocity fluctuations at $(1-r/R)=0.2$ and $Re_D=12\,500$, constructed using Taylor’s hypothesis. (a) Instantaneous fluctuations; (b) the first ten POD modes reconstructed and superimposed, creating a filtered velocity field. Flow is from left to right.

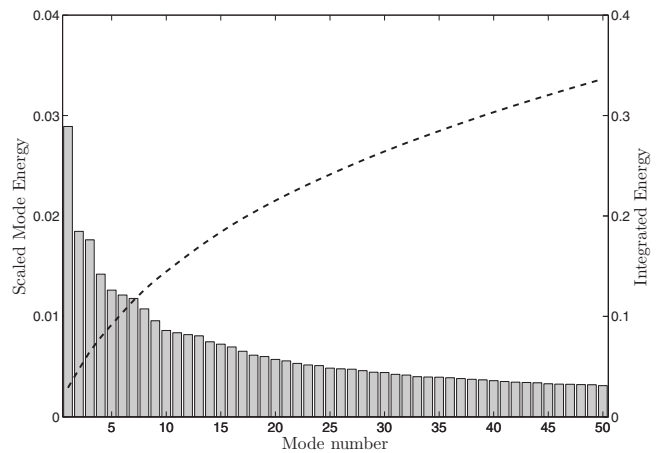


FIG. 3. Scaled energy content of the first 50 POD modes. The integrated turbulent kinetic energy with increasing mode number is shown by the dashed line.

Westerweel,¹⁶ modified to allow for arbitrary values of α_1 and α_2 .

The resolution of the data is about 2.15 vectors per mm^2 , and data near the wall (for $1-r/R < 0.1$) were discarded because of insufficient resolution caused optical refraction problems. Here, r is measured from the centerline.

Figure 2(a) displays the streamwise velocity fluctuations u_x at a wall distance $(1-r/R)=0.2$ using Taylor’s hypothesis. The velocity field is transformed to be viewed in Cartesian coordinates by unrolling the cylindrical plane. The distances are scaled with the pipe radius, and the velocity fluctuations are scaled with the friction velocity u_τ , where $u_\tau = \sqrt{\tau_w/\rho}$ and the wall stress τ_w is calculated from the pipe friction relationship given by McKeon *et al.*¹⁷ The high- and low-speed regions reveal the presence of the VLSM, and their general appearance is very similar to that observed in previous pipe flow studies.⁶

Snapshot POD was then performed on the three-dimensional fluctuating velocity data. Since the VLSMs are expected to be the most energetic structures in the flow, a superposition of the most energetic POD modes should identify their presence. Figure 2(b) shows the superposition of

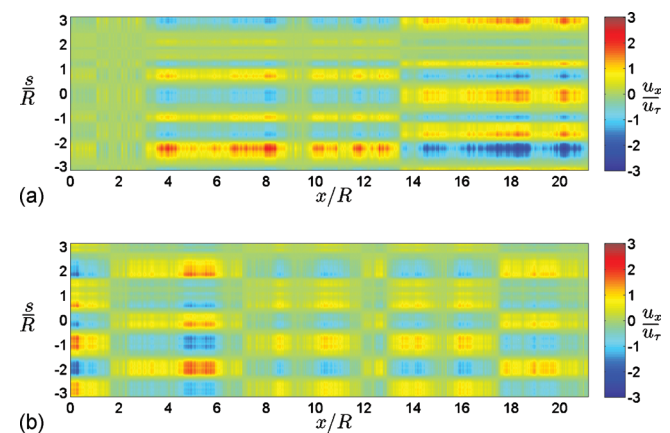


FIG. 4. (Color) The most energetic POD modes at $(1-r/R)=0.2$. (a) First mode; (b) second mode.

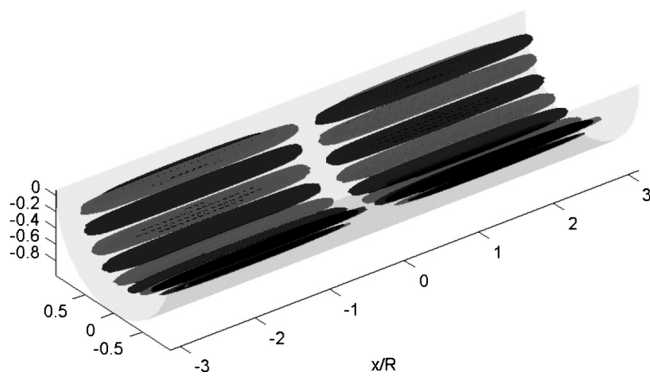


FIG. 5. Isocontours of positive and negative streamwise velocities for the sum of left- and right-going VLSM (helical) response modes obtained by linear stability analysis for $Re_D = 75 \times 10^3$. The azimuthal wavenumber was 10, and the streamwise wavenumber for each mode was 1. Figure adapted from Ref. 14.

the ten most energetic POD modes, and the relative energy content of the first 50 modes is given in Fig. 3. By comparing Figs. 2(a) and 2(b), it is evident that the first ten modes capture all the principal characteristics of the VLSM. This suggests that the VLSMs are constructed of the most energetic POD modes that, when superimposed, give the impression of large meandering structures.

To reveal this behavior more clearly, we can reduce the number of modes even further. Figures 4(a) and 4(b) show the reconstruction using only the first and second modes. The first reconstructed mode demonstrates coherence over a streamwise extent of about $10R$ with about nine modes around the circumference. Each set is azimuthally shifted half a period with respect to the previous one. The second mode has a streamwise extent of about $4R$, but again there are about nine modes around the circumference. Figure 5 shows the theoretical isocontours of the positive and negative streamwise velocities for the sum of left- and right-going VLSM response modes obtained by linear stability analysis.¹⁴ The periodicity of the modes for the theoretical and experimental works is in excellent agreement, although the streamwise extent of the theoretical predicted structures is somewhat shorter than the experimentally observed structures.

The rapid decrease in streamwise extent and the azimuthal phase shift between successive modes mean that, when superimposed, a meandering character appears even with a small number of modes. Figure 6 shows that the superposition of the first four modes already displays a highly meandering structure. A similar result is obtained by the su-

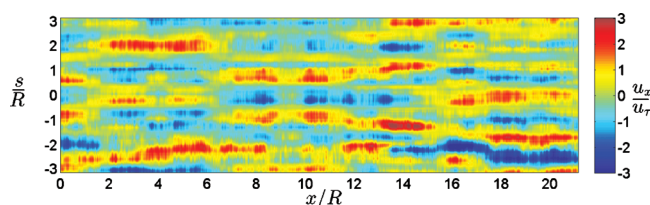


FIG. 6. (Color) Superposition of the first four POD modes at $(1-r/R)=0.2$, showing how long, meandering structures can be formed from a small number of modes.

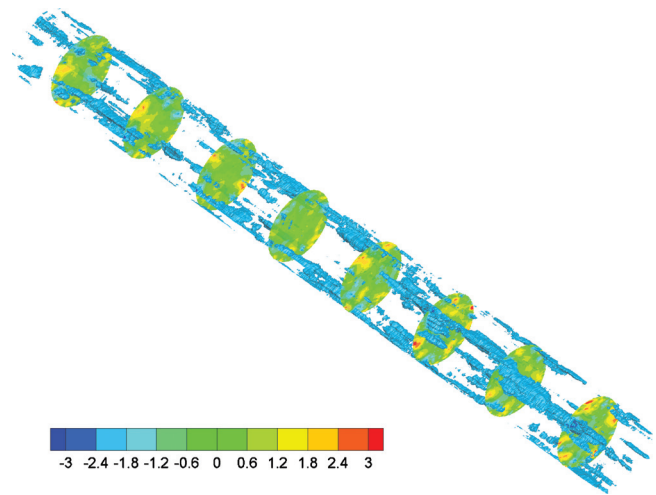


FIG. 7. (Color) Isosurfaces of the reconstructed streamwise velocity field below a threshold value of $u_x/u_r = -1.8$ using the first ten POD modes showing the three-dimensionality and the meandering behavior of the structures. It can also be seen how the structures are varying in size while meandering. The flow is from upper left to lower right.

perposition of a small number of linear stability modes (McKeon, private communication), providing further support for the linear perturbation origin of the VLSM.

The three-dimensional structure of the VLSM may now be visualized by using the first ten reconstructed POD modes. Figure 7 shows isosurfaces of the reconstructed streamwise velocity field of $u_x/u_r = -1.8$. The velocity distributions in the cross-stream planes have been added to show the alternating high- and low-speed regions. It can be seen how the structures are evolving both radially and azimuthally, and changing in size while doing so.

Figure 8 shows the isosurface of the VLSM seen when viewing upstream, emphasizing the radial extent of the low-speed structures. This indicates that the structures on occasion extend to the center of the pipe, demonstrating that, at least in pipe flow at this Reynolds number, the VLSMs grow larger than the logarithmic layer and interact with the outer layer, in contrast to earlier observations.³

The number of modes used to reconstruct the velocities is somewhat arbitrary, but the first few modes capture the

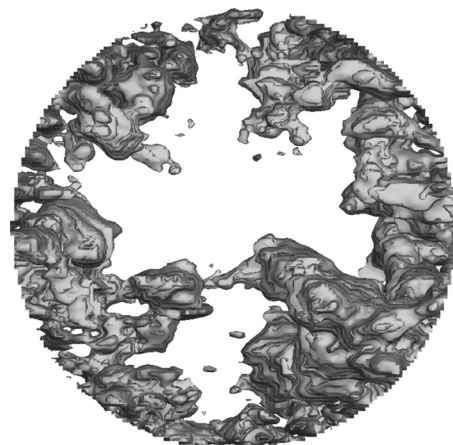


FIG. 8. Upstream view of the isosurfaces presented in Fig. 7.

general behavior well. Due to the procedure used when reconstructing velocities, it is difficult to determine the boundaries of a given structure. Following a single structure and discerning where it begins or ends is still, at this point, a subjective process.

It has been shown that the VLSM can be reconstructed using a small number of POD modes, and that the superposition of only the four most energetic modes will recreate meandering structures that appear to be much longer than any of its constituent modes. It appears that POD is a powerful tool for visualizing the three-dimensional character of the VLSM. The results strongly suggest a possible connection between the origin of the VLSM and linear stability analysis. The structures display a highly three-dimensional behavior where they meander both azimuthally and radially, and they may in some instances reach all the way from the buffer layer to the center of the pipe.

This work was supported under ONR Grant No. N00014-09-1-0263 (program manager Ron Joslin) and AFOSR Grant No. FA9550-09-1-0569 (program manager John Schmisser).

¹B. J. Balakumar and R. J. Adrian, "Large- and very-large-scale motions in channel and boundary layer flows," *Philos. Trans. R. Soc. London, Ser. A* **365**, 665 (2007).

²M. Guala, S. E. Hommema, and R. J. Adrian, "Large-scale and very-large-scale motions in turbulent pipe flow," *J. Fluid Mech.* **554**, 521 (2006).

³K. C. Kim and R. J. Adrian, "Very-large-scale motion in the outer layer," *Phys. Fluids* **11**, 417 (1999).

⁴A. J. Smits, B. J. McKeon, and I. Marusic, "High Reynolds number wall turbulence," *Annu. Rev. Fluid Mech.* **43**, 353 (2011).

⁵C. D. Tomkins and R. J. Adrian, "Energetic spanwise modes in the logarithmic layer of a turbulent boundary layer," *J. Fluid Mech.* **545**, 141 (2005).

⁶J. P. Monty, J. A. Stewart, R. C. Williams, and M. S. Chong, "Large-scale features in turbulent pipe and channel flows," *J. Fluid Mech.* **589**, 147 (2007).

⁷N. Hutchins and I. Marusic, "Large-scale influences in near-wall turbulence," *Philos. Trans. R. Soc. London, Ser. A* **365**, 647 (2007).

⁸S. C. C. Bailey and A. J. Smits, "Experimental investigation of the structure of large- and very-large-scale motions in turbulent pipe flow," *J. Fluid Mech.* **651**, 339 (2010).

⁹J. P. Monty, N. Hutchins, H. C. H. Ng, I. Marusic, and M. S. Chong, "A comparison of turbulent pipe, channel, and boundary layer flows," *J. Fluid Mech.* **632**, 431 (2009).

¹⁰M. Tutkun, W. K. George, J. Delville, M. Stanislas, P. B. V. Johansson, J.-M. Foucaut, and S. Coudert, "Two-point correlations in high Reynolds number flat plate turbulent boundary layers," *J. Turbul.* **10**, N21 (2009).

¹¹R. Mathis, N. Hutchins, and I. Marusic, "Large-scale amplitude modulation of the small-scale structures in turbulent boundary layers," *J. Fluid Mech.* **628**, 311 (2009).

¹²R. Mathis, J. P. Monty, N. Hutchins, and I. Marusic, "Comparison of large-scale amplitude modulation in turbulent boundary layers, pipes, and channel flows," *Phys. Fluids* **21**, 111703 (2009).

¹³J. C. del Álamo and J. Jiménez, "Linear energy amplification in turbulent channels," *J. Fluid Mech.* **559**, 205 (2006).

¹⁴B. J. McKeon and A. S. Sharma, "A critical layer framework for turbulent pipe flow," *J. Fluid Mech.* **658**, 336 (2010).

¹⁵B. J. McKeon (private communication).

¹⁶C. W. H. van Doorne and J. Westerweel, "Measurement of laminar, transitional, and turbulent pipe flow using stereoscopic-PIV," *Exp. Fluids* **42**, 259 (2007).

¹⁷B. J. McKeon, M. V. Zagarola, and A. J. Smits, "A new friction factor relationship for fully developed pipe flow," *J. Fluid Mech.* **538**, 429 (2005).